

MECH3900 Coursework 1 - Helicopter stabiliser wing

Harry Fotheringham 201419355 and Imaan Alvi 201417843

February 2024

Group 225



UNIVERSITY OF LEEDS

Contents

- 1 Introduction** **1**

- 2 Method** **1**
 - 2.1 Units 1
 - 2.2 Geometry 1
 - 2.3 Materials 2
 - 2.4 Loading and Boundary Conditions 2
 - 2.5 Design Change 3
 - 2.6 Verification 3
 - 2.7 Sensitivity Test 4

- 3 Results and Discussion** **4**
 - 3.1 Design Changes 4
 - 3.2 Verification 4
 - 3.3 Sensitivity Test 4

- 4 Assignment review** **5**

- A Appendix 1: Task 5** **7**
 - A.1 Theoretical beam model input values 7
 - A.2 A1.2 Simple beam Abaqus model input values 7
 - A.3 A1.3 Results from both simple beam models 7

- B Appendix 2: Task 6** **8**
 - B.1 Mesh cases 8
 - B.2 Displacement measure & post-processing 8
 - B.3 Tabulated results 8
 - B.4 Analysis 8

- C Appendix 3: Stabiliser Images** **10**

- D Appendix 4: Loading Calculations** **11**

1 Introduction

This report is going to examine whether the model generated is fit to represent a horizontal stabiliser of a helicopter. Then it will discuss the effect of adding a different number of spars through the centre of the helicopter stabiliser. It will examine the effect of the number of spars on the displacement of the stabiliser tip when pressure is applied underneath to simulate the effect of straight and level flight. As well as stress through the spar that results from the lift applied to the stabiliser. It will also determine whether placing a spar in front of the current spar would be more or less effective on the changing deformation.

To verify the Abaqus model, 2 prior tests have been completed. Performing these two tests allows comparison between the more accurate new model that represents the actual helicopter wing to a more simplified version that follows the general shape of the geometry. Initially, the stabiliser is modelled as a beam and analytical beam theory is used to compare the results. It also allows comparison with the design changes added to the model, confirming the new model's accuracy. One of these tests is a mesh convergence test which provides evidence of an accurate mesh size to choose for the model without compromising computational output. However, due to the simple nature of the model, compromising is not often required.

A sensitivity test is performed to quantify the errors that could occur due to input parameter choices as well as manufacturing equipment. Examined in this report is the thickness that the material is manufactured to. Specifically, the 1mm thick material, as well as the young modulus of the material. These were chosen as errors during manufacturing would potentially increase/decrease the thickness specified and it would be crucial to investigate the stress and displacement response of the stabiliser concerning this potential change. Stabilisers can also be made of different aerospace materials, and the Youngs Modulus therefore also alters which would henceforth change the properties of the stabiliser.

2 Method

2.1 Units

A standard unit system has been used for this analysis. The geometry is defined in mm and the pressures in MPa, for a consistent unit set the Forces will be in N. The advantage of using this system is that the post-processing and examination of the results will be much simpler as conversion between units is not required to read the result.

2.2 Geometry

The stabiliser that the geometry is representing is shown from various perspectives in Appendix C. The geometry has been approximated using a plate model part in Abaqus. The thickness is added to the correct sections to mimic the thickness of the metal and create a 3D part, without having to mesh over this 3D section. Using a plate model is advantageous as the mesh of the model can be much more accurate using smaller element sizes as there is no geometric thickness resulting in significantly fewer elements. Also, the computational time is much faster when performing the analysis due to fewer elements. However, it is recognised that using the plate model will cause a loss in accuracy to the model as further geometry like rivets becomes very difficult to implement following the same methodology.

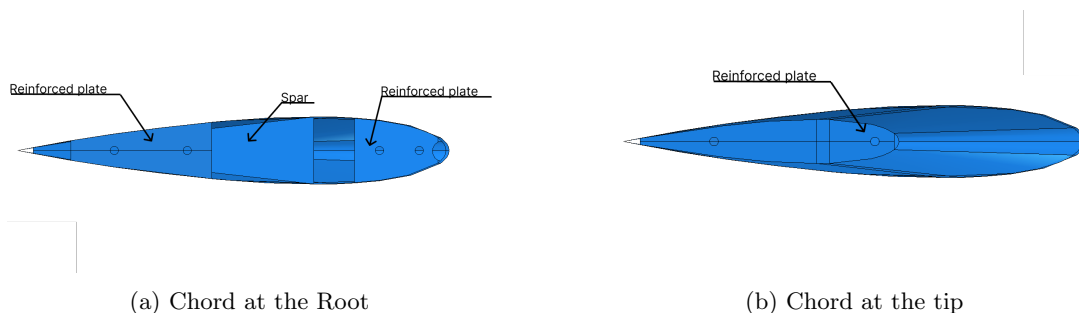


Figure 1: Shows a cross-sectional view of the wing at the tip and at the root of the stabiliser. 1b shows how the wing height tapers from the root to the tip.

Figure 12a shows the plate at the tip is located at the very outer edge of the wing and this has been copied over to the Abaqus replica. The plate at the tip has no suggestion of dimensions from the drawing therefore, it is assumed the plate extends right up to the bend on the trailing edge and behind the initial bend of the tip of the chord. There is no dimension given for the thickness of the plate so this has been assumed as 0.6mm like the rest of the rib plates. For the rib plates at the root of the stabiliser, an offset

from the root of 10mm has been chosen as the rivets are located 5mm from the edge according to the drawing so a value of 10mm for the plates seems reasonable.

These plates also have holes which have been included to increase the model accuracy, these create stress risers in certain planes in the model around the hole. By including them overall stress is more accurate. Some of the dimensions of these are not provided so the positions have been estimated using Figure 12a. It appears the holes are under the rivets marked on the drawings so these dimensions have been used. The hole on the root closest to the tip of the aerofoil has been placed 30mm in front of the other hole on the same metal plate as this looks similar to the images and since the displacement and stresses at the other end of the spar are being measured the placement of this hole will have minimal effect.

The reinforcing metal plates on the top and bottom surfaces have been replicated by making a partition line around their geometry and the model's thickness increased by combining the two plates. Some assumptions have been made to create the partition as not all of the dimensions required are present. This will be slightly different to having two separate features joined but provides an accurate representation in a plate model environment.

The spar is located correctly according to the drawing, rather than just the peak of each aerofoil, as is the case for the part used in the verification method shown in Appendix 1. This is an important feature to include in the model as this is the design change being made and will have a large effect on the deflection of the stabilizer tip and the stress along the spanwise direction of the stabiliser. The tapering of the stabiliser shown in Figure 11 has been included. Moving from root to tip the chord length and height will decrease. The chord length decreases from 260mm to 155mm and the chord height changes from 40.8mm to 24.8mm, the difference is clear in the model in Figure 1b. Also looking at the stabiliser in Figure 2 the angle at each side of the wing has been created to the specification.

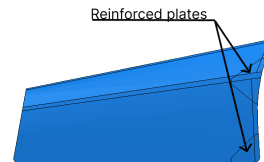


Figure 2: The outline of the wing with labels to detail the key features added to the wing.

Missing from the geometry are the rivets and brackets that link all the metal plates together.

These are difficult to implement in the plate environment. To counteract this missing feature the geometries are all combined as if they are fused as one piece of metal giving a similar effect as being joined by rivets. The rivets also created some deformation in the model which has not been incorporated as without dimensions this is complex to judge. Having the rivets in the model will create stress risers and as they are not included some accuracy will be omitted from the model however, as a local stress directly related to the rivets is not being measured the missing rivets effect will be negligible.

2.3 Materials

The material used for all of the metal is aviation aluminium as stated on the drawings. This material has a young modulus of 69 GPa and a poisons ratio of 0.3. The metal has also been assumed to be entirely elastic. This is a valid assumption because aviation alloys have high Elastic Moduli and high tensile strength [1], and since the pressures applied are relatively low it is safe to assume that the deformation will be elastic.

2.4 Loading and Boundary Conditions

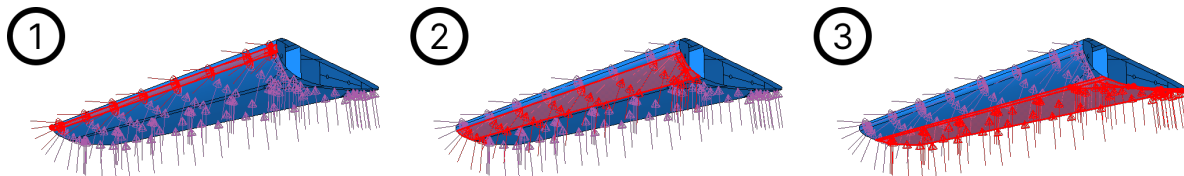
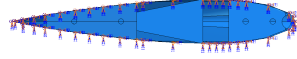


Figure 3: The three different sections of the wing where the three pressure loads have been applied in the model.

The load has been applied to the underside of the wing at the three panels shown in Figure 3. A pressure load has been used to mimic the effect of the stabiliser subjected to the loads of a real-life flight situation. Loads of 0.00306MPa, 0.00368Mpa and 0.000903MPa have been used for sections 1, 2 and 3 respectively.

Applying the loads in this way assumes that there is a constant pressure over each of the three regions. However, in reality, the pressure distribution over the aerofoil changes constantly along the chord-wise direction this is shown in Figure 14. The first section is designed to represent the pressure at the stagnation point. The second section contains the highest pressure where the suction peak on the aerofoil is generated and where the pressure increases until the peak of aerofoil thickness. The final section has the smallest pressure and is assumed to be uniform to the tip and this section covers the pressure decrease along the aerofoil. For the full load calculations see Appendix D.



On typical helicopters, stabilisers are attached and fixed in place. To simulate this situation, the Encastre condition is used along the edge of the root chord as can be seen in Figure 4.

Figure 4: The section of the model is constrained by the Encastre Boundary condition.

2.5 Design Change

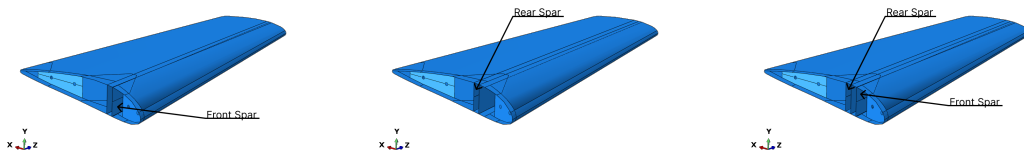


Figure 5: Design changes investigated with a front spar, rear spar and three spars

The number and position of spars through the centre of the wing have been changed and experimented with to discover what effect this will have on the stabiliser. It was predicted that changing the number of spars would cause less displacement at the tip and less deformation between the top and bottom plates due to the added structural support of the extra spars. However, the degree of this effect is unknown. This simulation will quantify the effect of the spars. If significant then it may be worth further research to determine whether having an extra spar or indeed multiple spars added to the stabiliser could prevent failure. Ultimately this could potentially have the ability to reduce the chance of failure and crashing due to a fault or malfunction from the stabiliser.

The spars have been added in parallel to the original spar. They have been maintained towards the centre of the model so they don't intersect the reinforcing plates. One spar has been added in front of the current spar and one behind. It is expected that having more spars will decrease the stress felt by the central spar and decrease the displacement of the tip. It will also explore whether there is a more favourable side to add the spar to.

2.6 Verification

The first verification process undertaken determines whether the computational model accurately represents the underlying mathematical model and its solution [2]. This is done by comparing a theoretical beam model which assumes a constant cross-sectional area, constant second moment of area and constant distributed load to a simple beam Abaqus model which uses a spatially 3D model with 1D beam elements as well as the same assumptions as the theoretical model. After conducting both calculations and analysis the deflection at the tip and the maximum stress are obtained from the values shown in Appendix 1. The values align very closely as they are very similar with a percentage difference of 3.7% for the deflection at the tip and 0.77% for the maximum stress. This verifies that the computational model can accurately represent the mathematical model.

The second verification process determines whether a model implementation accurately represents the conceptual description and solution to the model [3]. This was carried out through a mesh convergence and mesh error approximation on a simpler model of the stabiliser. The details of this are outlined in Appendix 2 where we observe that as the mesh is refined, i.e., the mesh size decreases, the change in displacement also decreases as the displacement value moves closer to one value (the true value) and from the graph in Appendix 2, there is a clear strong convergence pattern with a decrease in the change in displacement for each case.

A similar mesh convergence test on the simpler model has been used for the stress on the model. The results of this test are shown in Figure 7. This is completed to check the results align with the

displacement mesh convergence showing that using a similar mesh size for both cases is an accurate representation.

2.7 Sensitivity Test

Sensitivity analysis is carried out to assess the influence of the various input parameters of the Abaqus model on certain outputs. The tests being performed here are to investigate the effect of altering the thickness of the model. The thickness is altered between 0.85 - 1.15 in increments of 0.05 with thickness of 1mm for the base model and the Von Mises Stress and displacement in the y direction are observed. The other sensitivity test involves altering the Youngs modulus of the stabilizer to reflect different material choices used to make the stabilizer in real-life applications. This is another great use case of sensitivity tests to quantify the results of these uncertainties. It is also possible that the thickness of the model is milled slightly smaller or slightly larger due to machine tolerance. The Youngs modulus for each alloy is indicated in brackets; Base model (69 GPa), 2024-T4 (73.1 GPa), 5052-H32 (70.3 GPa), 6061-T6 (68.9 GPa), 7075-T6 (71.7 GPa) [4].

3 Results and Discussion

3.1 Design Changes

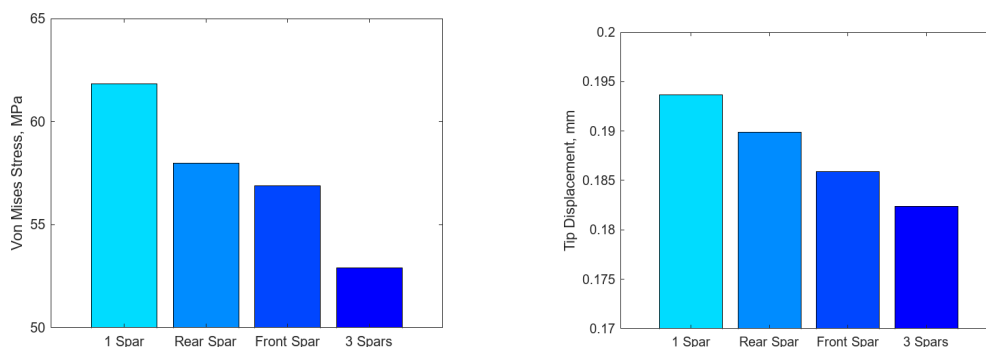


Figure 6: Von Mises Stress and displacement in y direction as a result of the design changes

Figure 6 outlines the Von Mises stress and displacement in the y direction for our selected design changes. A decrease in both Von Mises stress and displacement can be observed with the addition of spars. The percentage difference in comparison to the base model is 1.97%, 4.02% and 5.82% for the rear spar, front spar and 3 spars respectively indicating a minor effect on displacement with the addition of spars. The Von Mises stress on the other hand had a slightly bigger difference with the addition of spars with the addition of 3 spars yielding a percentage difference of 14.5% with a decrease of approximately 10 MPa. The addition of the front and rear spar however did not yield much difference with an 8.0% and 6.2% percentage difference respectively.

3.2 Verification

This verification test shows similar results to the other mesh convergence test outlined in Appendix 2. Figure 7 suggests that the mesh cases of 128 and 64 are inaccurate and not representative of the actual stresses as there is very little difference between the two. From this point onwards moving from the 64mm element size to the 2mm element size there tends to be a decrease in the difference between the mesh cases. After reaching an element size of 8mm the difference becomes less than 0.4MPa. For this reason and the reasoning explained in Appendix 2 a global mesh size of 8mm was chosen for the model. This choice resulted in a mesh error of 0.8154 relatively low compared to the 60MPa stresses in the model.

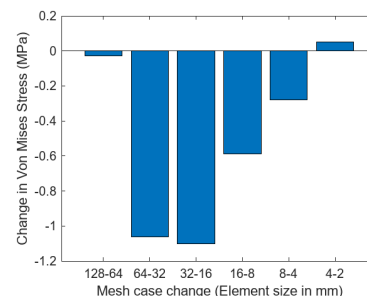


Figure 7: Global Mesh convergence test for the Von Mises Stress on a simplified model.

3.3 Sensitivity Test

Figure 8 outlines the variation in Von Mises stress when the thickness is altered between 0.85 and 1.15. We observe a gradual decrease in the Von Mises stress with increasing thickness which was expected as an

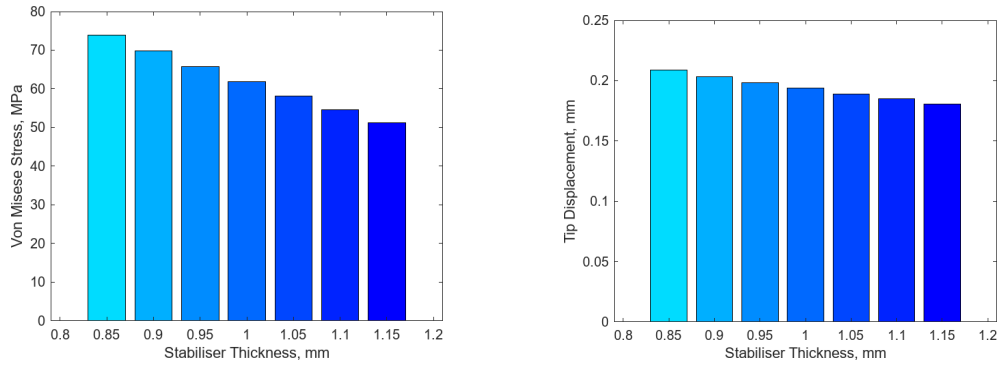


Figure 8: Test 1 - altering thickness and observing the resulting Von Mises Stress and displacement in y direction

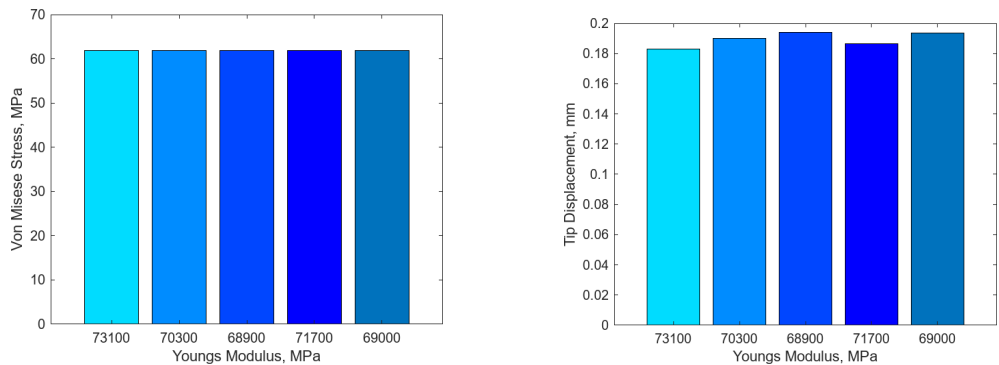


Figure 9: Test 2 - altering Youngs Modulus and observing the resulting Von Mises Stress and displacement in y direction

increased thickness leads to the stiffness of the body increasing which decreases the stress intensity factor. There is a percentage difference of 19.7% between the base model and the lowest thickness (0.85 mm) and a percentage difference of the highest thickness (1.15 mm) and the base model is 17.1% which is acceptable. Increasing the thickness also gradually decreases the displacement (in the y direction) as outlined in figure 9. Since the stiffness has increased the deflection of the component under the given load decreases whereby the percentage difference between the lowest thickness (0.85 mm) tested and the base model is 7.77% and the percentage difference between the highest tested thickness (1.15 mm) and the base model is 6.72% which is also acceptable. Figure 9 outlines the variation in Von Mises stress and displacement in the y direction by altering the Youngs Modulus. The Von Mises stress remains the same as that of the base model for each Youngs Modulus tested. On the other hand, the displacement in the y direction displays a different pattern. Greater Youngs modulus values of 70.3, 71.7 and 73.1 GPa elicit lower displacement values with percentage errors of 1.8%, 3.8% and 5.6% respectively (in comparison to the base model). The sensitivity tests carried out allow us to conclude that there isn't much of a difference when utilising different aerospace materials (different Youngs moduli) as well as if there were errors during manufacturing that would alter the thickness and henceforth the stabiliser is fit for purpose and the yield point will not be exceeded.

4 Assignment review

The undertaken assignment was largely successful. We had allocated an equal amount of time for most of the steps; however, we encountered unexpected complexity with the model, leading to a need for additional time on this step, which became the most challenging aspect. Fortunately, we could compensate by completing the other, more straightforward tasks. The original plan included three sensitivity tests, but time constraints only allowed us to complete two, however this fit within the brief provided and we found these two adequate for assessing potential errors. Conducting the sensitivity tests was the most enjoyable aspect, as we observed the impact of small changes as well as being able to speculate on how this would relate to real-life applications. In hindsight, a more tailored allocation of time to tasks based on their level of complexity would have been beneficial to ensure timely completion and possibly allow for additional sensitivity tests and a broader exploration of results in future iterations of this assignment.

References

- [1] R. Raj, P. Selvam, and M. Pughalendi. "A Review of Aluminum Alloys in Aircraft and Aerospace Industry". In: (June 2021).
- [2] ASME V&V. "Guide for Verification in Computational Solid Mechanics". In: (2006).
- [3] Ellis & Weiss Anderson. "Computer Methods in Biomechanics & Biomedical Engineering". In: (2007).
- [4] MatWeb. "MatWeb: Online Materials Information Resource". In: (2024). Accessed: 01/02/2024.

A Appendix 1: Task 5

A.1 Theoretical beam model input values

Structural parameters	Value
Units	mm, kN, mm ² , mm ⁴
Spanwise length of stabiliser	550
Cross sectional profile representation (i.e. how many sections were used to describe the curves)	45
Thickness of the stabiliser skin	1
Total area of the cross-sectional profile at the mid-point of the span	428.2
Centroid position within the cross-sectional profile (coordinates)	(101.5552,0)
Second moment of area of the cross-sectional profile at the mid-point of the span	63311.283
(Other) Theoretical beam inputs	Value
Young's modulus	69 GPa
Load per unit length	350 N/m
Max moment	52.9375
Y-position of max stress	16.6004 mm

A.2 A1.2 Simple beam Abaqus model input values

Input	Either value or a brief description
Units system	mm, GPa, kN
Beam length	550mm
Element type (inc. shape function)	Beam type. Linear with lots of elements. This could be changed to have much fewer elements with a cubic shape function.
Number of elements	550
Young's modulus	69GPa
Boundary conditions	At one edge of the beam, entirely constrained (encastre) as we are assuming that this is a cantilever beam and the stabiliser is fixed on one edge of the helicopter
Applied load	350N/m or 0.00035kN/mm
Cross sectional profile implementation method.	Created an Arbitrary Profile of all of the coordinates from the excel spreadsheet provided for maximum accuracy

A.3 A1.3 Results from both simple beam models

Output	Theoretical beam model	Abaqus beam model
Deflection at the tip	0.916428	0.951668 mm
Maximum stress	13.8702	13.7632 MPa

B Appendix 2: Task 6

B.1 Mesh cases

Global seed size (mm)	Minimum edge length (approx.)	Maximum edge length (approx.)	Total number of elements	Total number of nodes
128	5.31748	1.95711e+02	32	34
64	5.31748	9.79927e+01	76	76
32	5.31748	3.92083e+01	272	272
16	2.71508	2.17831e+01	1023	1020
8	2.71508	9.80242	3770	3762
4	2.71508	5.02689	14820	14803
2	1.49840	3.68857	59052	59020

B.2 Displacement measure & post-processing

We are measuring the displacement in the U2 (y) direction in mm. To extract this information from Abaqus we changed the output displacement dropdown to select the U2 direction and chose which node we wanted to measure the displacement from. We chose to measure the displacement on the node directly below the centre of the spar, at the furthest distance from the wing root or the wing tip. To extract the data for this point we used the query tool inside Abaqus to inspect the node selected. The units were consistent and in mm or MPa allowing for easy comparison and post processing.

B.3 Tabulated results

Global seed size (mm)	Displacement (mm)	Change in displacement from lower to higher resolution (mm)
128	0.678052	N/A
64	0.503142	0.174910
32	0.428541	0.074601
16	0.402771	0.025770
8	0.398095	0.004676
4	0.396039	0.002056
2	0.395532	0.000507

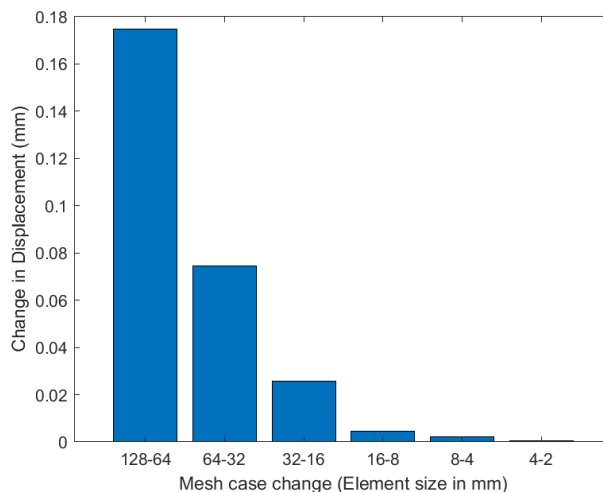


Figure 10: Global Mesh convergence test for the displacement on a simplified model.

B.4 Analysis

From the figure above, a pattern can be observed between the seed cases. As the mesh is refined, i.e., the mesh size decreases, the change in displacement also decreases as the displacement value moves closer to one value (the true value) and the results stabilise with increasing mesh density therefore a convergence pattern can be witnessed. From the graph, there is a clear strong convergence pattern with a decrease in the change in displacement for each case.

We will use the 8mm mesh because it has a small difference between the previous value and the next value. If we wanted to make the mesh size smaller, it would have a significant effect on the time that it takes to complete a job as the number of nodes jumps from 3770 to 14820. Therefore, an 8mm mesh case would not use too much computing power or cost making it suitable for additional modelling work. If we move past 8mm mesh to 4 mm the difference is very slight which would require extra computing power and the result would overall not be of much greater accuracy. There is also some extra room with the 8 mm mesh case for adding more local nodes to specific areas of interest while being able to remain under the 250,000 node limit.

The residual mesh error is 0.007239 mm by adding the change in deflection between our chosen mesh case (which is 8 mm) and the following mesh cases (4 and 2 mm)

C Appendix 3: Stabiliser Images



Figure 11: Top down view of the Helicopter Stabiliser wing showing the spanwise direction and shape.



(a) Wing tip



(b) Wing Root

Figure 12: Helicopter Stabiliser wing chords. The internal plate geometry present in the wing at both the tip and the chord can be seen here.

D Appendix 4: Loading Calculations

The Aerofoil used is the NACA 0016 Aerofoil. Figure 13 provides verification that the plot matches the NACA 0016 Aerofoil.

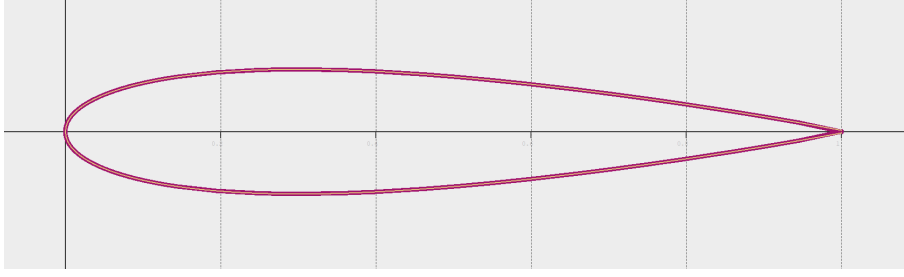


Figure 13: The red line shows the plotted coordinate of the actual aerofoil and the orange line shows the NACA 0016 Aerofoil. Both are normalised between 0 and 1.

Also provided is a C_P plot which is shown in Figure 14. The velocity has been assumed to be 49 m/s

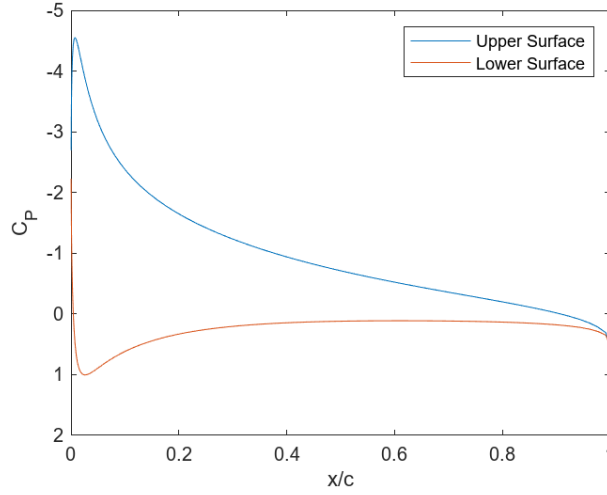


Figure 14: Pressure Coefficient plot along the Chord of the helicopter stabiliser (NACA 0016 Aerofoil).

Air Density (kg/m ³)	Velocity (m/s)	Chord Length (m)	Span Length (m)
1.13	49	0.2075	0.512

Table 1: Constant values used for each of the panels to calculate the pressure

and the density has been estimated using the International Standard Atmosphere value and an altitude of 2500m for the flight the air density is 1.13 kg/m³. Due to the complex shape of the stabiliser used in this analysis to calculate the loads the simpler model used for the displacement mesh convergence was used. The Chord Length and Span Length have been averaged across this simplified stabiliser.

$$C_l = \int_{x_1}^{x_2} (C_{pl}(x) - C_{pu}(x)) dx \quad (1)$$

By using the C_P plot and Equation 1 3 lift coefficients can be found and are shown in Table 2. Equation 2 is used to find the load per unit span length with a known lift coefficient.

$$\omega = \frac{1}{2} \rho V^2 C_l c \quad (2)$$

	Lift Coefficient	Load per unit span length (N/m)	Total Load (N)	Area (m ²)	Pressure (Pa)	Pressure (MPa)
Panel 1	0.081439	22.924	11.737	0.003831	3063.715	0.003063715
Panel 2	0.658392	185.329	94.888	0.025761	3683.411	0.003683411
Panel 3	0.501957	141.295	72.343	0.080111	903.032	0.001631379

Table 2: Collection of data used to calculate the pressure to be used for the loads on the stabliser.